Water Resources Research

RESEARCH ARTICLE
10.1029/2020WR027158

Understanding the Asymmetry of Annual Streamflow Responses to Seasonal Warming in the Western United States

Zhaoxin Ban[1], Tapash Das[2], Dan Cayan[2], Mu Xiao[1], and Dennis P. Lettenmaier[1]

[1]Department of Geography, University of California, Los Angeles, Los Angeles, CA, USA, [2]Scripps Institution of Oceanography, University of California, San Diego, La Jolla, CA, USA

Key Points:
- Streamflow responses to warm versus cool season warming for four major Western United States basins are mostly consistent across four models
- Evapotranspiration to temperature sensitivity dominates the asymmetry of streamflow reductions under warm versus cool season warming
- Differences in the basins' runoff responses to seasonal warming are mainly associated with seasonal gross incoming water and temperature

Supporting Information:
- Supporting Information S1

Correspondence to:
D. P. Lettenmaier,
dlettenm@ucla.edu

Citation:
Ban, Z., Das, T., Cayan, D., Xiao, M., & Lettenmaier, D. P. (2020). Understanding the asymmetry of annual streamflow responses to seasonal warming in the Western United States. *Water Resources Research*, *56*, e2020WR027158. https://doi.org/10.1029/2020WR027158

Received 17 JAN 2020
Accepted 10 NOV 2020
Accepted article online 17 NOV 2020

Abstract The response of annual runoff volume to sub-annual climate warming is highly uncertain, and the governing mechanisms remain poorly understood, challenging adaptive water management. A typical exemplar is the Western United States, where climate models project substantially stronger warming in the warm season (April to September) than in the cool season (October to March). We investigate the asymmetrical responses of annual and seasonal streamflow changes to warm season and cool season warming for four regionally important basins in the Western United States using an ensemble of four land surface (hydrological) models. Our results show that (i) the general features of seasonal and annual streamflow responses to asymmetrical warming are consistent across models, although the magnitudes vary. The multi-model mean shows annual runoff declining from 2.0% up to 7.5% under 3°C warm season warming, and from 2.2% up to 4.7% under 3°C cool season warming across the four basins. (ii) The asymmetry of the seasonal evapotranspiration sensitivity to temperature constrains the asymmetry of annual streamflow responses to seasonal warming; and (iii) basins with characteristics such as high ratios of warm to cool season gross incoming water, cooler summers, and colder winters have the strongest relative annual streamflow decreases for warm season warming relative to cool season warming. The pattern in (iii) is explained by the variation of evapotranspiration-temperature sensitivity in response to a compound set of processes, including the enhanced rate of water holding capacity increase with warmer temperatures, temperature-related snowmelt-albedo feedback, and enhanced surface resistance with warmer temperatures.

1. Introduction

The Western United States, one of the most rapidly growing parts of the country, is also its driest region. Much of the water consumed in the region comes from snowmelt (Li et al., 2017), a source experiencing significant volume and timing fluctuations as the climate of the region warms (Mote et al., 2005, 2018). These fluctuations in the snowpack are usually accompanied by changes in the region's annual streamflow, motivating efforts to understand the mechanisms dominating the region's streamflow volumetric response to climate warming.

Many previous studies have examined both historical changes and future projections of the region's streamflow (e.g., Gergel et al., 2017; Hayhoe et al., 2004; Kim & Jain, 2010; Stewart et al., 2005). These studies have generally found that warmer temperatures will lead to reduced winter snowfall and increased rainfall, earlier snowmelt, and hence earlier seasonal peak runoff in the year. These phenomena are primarily a consequence of cool season (October to March) warming (Hamlet et al., 2005; Knowles et al., 2006; Mote et al., 2005). However, evaporative demands are larger in the warm season (April to September) than in the cool season, and climate models mostly project more warming in the warm season than in the cool season over much of the Western United States (Hayhoe et al., 2004). These facts raise questions about how the changes in the warm season will affect the region's hydrology, especially annual streamflow volume changes.

Das et al. (2011) investigated the annual streamflow sensitivity to cool and warm season warming using a single model simulation (variable infiltration capacity model [VIC], Liang et al., 1994) across four regionally important river basins in the Western United States. They showed that warm season warming generally leads to more significant decreases in annual streamflow than cool season warming across the four

basins, highlighting the importance of both seasons' warming effects on the sensitivity of Western United States streamflow to climate warming. Two other recent papers (Vano et al., 2015; Vano & Lettenmaier, 2014) investigated the sensitivity of Western United States streamflow to temperature change on a seasonal scale and found substantial negative streamflow changes in response to warming. Like Das et al. (2011), they performed simulations with a single model (also VIC) to study how streamflow responds to warm and cool season warming. Furthermore, they focused more on quantifying the change than on understanding the changes in the hydrological processes. Based on these studies, we find two main motivating questions that remain unanswered: first, are the predictions of "how" the region's streamflow will change in a warming climate model-dependent, and second, "why" the streamflow responses to seasonal warming show the seasonally dependent sensitivities documented in Das et al. (2011).

To address the two questions, we first investigate the streamflow response patterns to seasonal warming over the four river basins using VIC and three other hydrology models (described in sections 2, 3.1, and 3.2). Then we identify the dominant factors controlling annual streamflow responses to seasonal warming using a water balance framework (described in sections 3.3–3.5). The method to investigate mechanisms controlling those dominant factors of streamflow response is in section 3.6. Results are in section 4, with discussion and conclusions in sections 5 and 6, respectively.

2. Study Area

Our study domain consists of the same four regionally important Western United States river basins as in Das et al. (2011): the Columbia Basin; the Upper Colorado Basin (hereafter Colorado); California's Northern Sierra Nevada (N. Sierra); and California's Southern Sierra Nevada (S. Sierra). For the Columbia Basin, we consider the naturalized flows above the Dalles, OR, obtained from the Bonneville Power Administration (2019); for the Colorado basin, we consider the naturalized flows of the Colorado River above Lees Ferry, AZ, obtained from The U.S. Bureau of Reclamation (USBR, 2018); for the N. Sierra, we use the sum of flows from gauges designated SBB, FTO, and YRS; for the S. Sierra, we use the sum of flows from gauges named MRC, SJF, SNS, and TLG. We obtained both N. Sierra and S. Sierra's unimpaired flow data (Bay-Delta Office, California Department of Water Resources, 2007) from the California Data Exchange Center (2018, http://cdec.water.ca.gov/dynamicapp/QueryWY). Details of the gauges' full names and data sources are in Table 1.

Based on the locations of stations providing naturalized flows, we delineated the four basin masks using a data set of river channel network (Wu et al., 2012), as applied in Xiao et al. (2018). Comparisons between model-simulated monthly hydrographs and observations are in supporting information Text S1 and Figure S1.

3. Data and Approach

3.1. Forcing and Models

We used the Livneh (L13) meteorological forcings (Livneh et al., 2013) to drive VIC version 4.1.2 (Liang et al., 1994), the community Noah LSM with multi-parameterization options (hereafter Noah-MP) (Niu et al., 2011; Yang et al., 2011), the Sacramento Soil Moisture Accounting model (SAC-SMA) (Burnash et al., 1973), and the Catchment model (Koster et al., 2000). The L13 forcing was extended through 2018 (available to be downloaded from ftp://livnehpublicstorage.colorado.edu/public/sulu) so that the data set covers 1915 through 2018 at a daily time-step over the entire conterminous United States (CONUS) domain (at 1/16 lat-long degree spatial resolution). The L13 data contain four primary time-varying forcing fields: daily precipitation, maximum daily temperature (Tmax), minimum daily temperature (Tmin), and surface wind speed. The first three are interpolated from daily weather station observations, while surface wind speed is interpolated from atmospheric reanalysis data (Kalnay et al., 1996; Livneh et al., 2013).

We applied all four models over the four basins for the period 1916 to 2018, using the water year 1915 as spin-up (10 times). Similar to Das et al. (2011), we ran VIC in the water balance mode, which means that surface temperature is set to the surface air temperature for purposes of computing surface energy fluxes. We used VIC parameters from L13 to ensure consistency between model parameters and forcings

Table 1
Stream Gauge (or Location) Names and Data Sources

Basin	Gauge location(s) or tributaries	Data source
Columbia	The Dalles	Bonneville Power Administration (BPA): https://www.bpa.gov/p/Power-Products/Historical-Streamflow-Data/Pages/No-Regulation-No-Irrigation-Data.aspx)
Colorado	Lees Ferry	U.S. Bureau of Reclamation (USBR): https://www.usbr.gov/lc/region/g4000/NaturalFlow/current.html
N. Sierra	The sum of the Sacramento River above Bend Bridge (SBB), The Feather River at Oroville (FTO), and The Yuba River near Smartville (YRS)	California Data Exchange Center (CDEC): http://cdec.water.ca.gov/dynamicapp/QueryWY
S. Sierra	The sum of the Stanislaus River at Goodwin (SNS), The Merced River near Merced Falls (MRC), The Tuolumne River at LA Grange Dam (TLG), and the San Joaquin River Below Friant Dam (SJF)	

(calibrated by Maurer et al., 2002, and subsequently by Livneh et al., 2013), and therefore we did not perform additional parameter estimation/calibration for VIC. We disaggregated the daily forcings (to hourly and 3-hourly) using the Mountain Microclimate Simulation Model (MTCLIM) algorithms (Bohn et al., 2013) incorporated in VIC to estimate downward shortwave and longwave radiation, relative humidity, specific humidity, and surface atmospheric pressure. We also used the hourly disaggregated forcings as inputs to the Noah-MP model, and 3-hourly disaggregated forcings as inputs to the Catchment and SAC-SMA models. For the partitioning of precipitation between rain and snow, we used the Jordan 91 option in Noah-MP and default settings in the other three models. We computed potential evapotranspiration (PET, a required input to SAC-SMA) from 3-hourly VIC disaggregated forcing variables using the Penman-Monteith algorithm (to produce reference ET, or ET_0, which was used as a surrogate for PET) based on the UMD vegetation classification scheme (2020, description and data: https://ldas.gsfc.nasa.gov/nldas/vegetation-parameters). We then calibrated the PET adjustment parameter (PEADJ) in SAC-SMA, to make the output long-term climatological hydrographs approach the observed ones (Figure S1). Additionally, because the models cannot represent the horizontal movement of glaciers, in VIC, we reset SWE to zero on 1 September at every grid cell to avoid the continuous accumulation of SWE in some cold grid cells (mostly in the North Cascades), which are usually covered by glaciers in the real world. We only reset SWE for VIC because VIC tends to cause more pixels to have abnormally high SWE accumulation than other models, while other models' over-year accumulated SWE only happens at very few pixels and has a negligible effect on our basin-scale discussion.

3.2. Temperature Warming Scenarios

We isolated the effect of asymmetrical warming on runoff by conducting precipitation-fixed warming experiments as in Das et al. (2011). Das et al. (2011) found that by the end of this century, the Coupled Model Intercomparison Project Phase 3 (CMIP3, Maurer et al., 2007)-projected annual average warming across the four basins is about 3°C and hence applied 3°C warming in their experiments. We rechecked the projected warming magnitude with Coupled Model Intercomparison Project Phase 5 (CMIP5, Reclamation, 2014) (Figure S2), model selection (see Text S2 and Table S1) ensemble average (averaged over 10 best global models for the regions as suggested by Rupp et al., 2013, and California Department of Water Resources, Climate Change Technical Advisory Group, 2015), and found that the mid-century projected warming (2035–2065 as compared with 1976–2005 as defined in Pierce et al., 2018, which is a presumably more important time period for water management than end of century) across the four basins for RCPs 4.5 and 8.5 are mostly under or around 3°C. Therefore, we adopted the same seasonal warming scenario as in Das et al. (2011), adding 3°C to the entire year, the warm season, and the cool season separately. Since our focus is on the runoff-temperature sensitivity rather than forecasting the actual runoff response, we opted for constant warming magnitudes.

Addition of 3°C warming (or any other constant) to both the daily maximum and minimum temperatures assures that the downward solar radiation produced by the MTCLIM model, which is based on the daily

temperature range, is unchanged. Downward and emitted longwave radiation do change (slightly) as they are related to daily average temperatures (see Bohn et al., 2013, for details).

3.3. Measure of Annual Streamflow Response Asymmetry to Seasonal Warming

Here we use the symbols (see also Table S2) ET for evapotranspiration, Q for streamflow, P for precipitation, T for temperature, SM for soil moisture, and SWE for snow water equivalent. For terms of the form $X_{a,w3d}$, the first subscript indicates the period (a: annual, w: warm season, c: cool season) and the second subscript is the warming scenario (w3d: warm season warming 3°C, c3d: cool season warming 3°C or b: baseline). ∂X, dX, and ΔX all represent the value of variable X under warming scenarios minus the baseline value. $\overline{X}$ represents the long-term climatology of variable X averaged across the historical period (1916–2018).

According to the water balance equation (Equation 1),

$$P - ET - Q = \Delta SM + \Delta SWE \tag{1}$$

when P is fixed (as in our experiments), and when the change of long-term SM and SWE is negligible over the multi-decade period of analysis, the change of annual ET equals the change of annual Q (Equation 2).

$$\Delta ET = -\Delta Q \tag{2}$$

Therefore, the differential annual Q response to seasonal warming can be explained by the reasons that cause differential annual ET response to seasonal warming. It is easier to understand the annual Q response from the perspective of ET rather than from the complicated precipitation-snowmelt-infiltration-saturation process of Q generation, since ET is a more "instant" and "local" process with no time-lag and no spatial movement, and has a cleaner seasonal partition than Q. Here, we quantify the relative strength of annual ET response to warm versus cool season warming using a term $Pref_{ET}$. $Pref_{ET}$ (Equation 3) is defined as annual ET change under warm season warming ($\overline{ET_{a,w3d}} - \overline{ET_{a,b}}$), divided by the annual ET change under cool season warming ($\overline{ET_{a,c3d}} - \overline{ET_{a,b}}$).

$$Pref_{ET} = \frac{\overline{ET_{a,w3d}} - \overline{ET_{a,b}}}{\overline{ET_{a,c3d}} - \overline{ET_{a,b}}} \tag{3}$$

$Pref_{ET} > 1$ indicates that a basin has a larger annual ET change under warm season warming than under cool season warming, and $0 < Pref_{ET} < 1$ indicates the opposite. In short, when $Pref_{ET}$ is positive, the larger $Pref_{ET}$ is, the stronger "preference" for a basin to have stronger annual ET increase (streamflow decrease) under warm versus cool season warming. $Pref_{ET}$ can also be negative, which means that annual ET decreases under cool season warming but increases under warm season warming, indicating a larger annual ET increase (streamflow decrease) under warm season warming than under cool season warming.

Similarly, we can define a basin's "preferred" seasonal tendency for annual streamflow change under warm versus cool season warming, $Pref_Q$ (Equation 4).

$$Pref_Q = \frac{\overline{Q_{a,w3d}} - \overline{Q_{a,b}}}{\overline{Q_{a,c3d}} - \overline{Q_{a,b}}} \tag{4}$$

$Pref_{ET}$ should (approximately) equal $Pref_Q$ since we expect the sum of annual ET and annual Q to be constant (annual precipitation) under different warming scenarios, and this is confirmed in section 4.2.

3.4. Estimation of Pref Rank Across Basins

We use the ratio of ET change in the warmed season under warm versus cool season warming to estimate the relative rank of $Pref_{ET}$ across basins.

$$\text{rank}(Pref_{ET}) = \text{rank}\left(\frac{\overline{ET_{w,w3d}} - \overline{ET_{w,b}}}{\overline{ET_{c,c3d}} - \overline{ET_{c,b}}}\right) \tag{5}$$

One assumption embedded in Equation 5 is that ET changes within the warmed season dominate the annual ET change. We later confirm (in section 4.4) that the ET changes in the warmed season are

mostly caused by increasing evaporative demand associated with warming temperature, rather than water availability changes. Therefore, the ET change ratio in Equation 5 also represents the ratio of ET-T sensitivity.

3.5. Identification of the ET-T Sensitivity Variation

On a multi-model mean basis, we identified the basin characteristics that best constrain the variation of ET-T sensitivity by (i) calculating the Pearson correlations ($p = 5\%$) between normalized yearly data of five selected basin characteristics and ET-T sensitivity within each of the four basins, (ii) comparing the rank of the basin characteristics and corresponding seasonal ET-T sensitivities across basins, and (iii) visualizing the pattern on a pixel-by-pixel basis.

3.6. Attribution of ET-T Sensitivity Variation

We quantified the attribution of ET-T sensitivity based on the original Penman-Monteith model (Equation 6) (Allen et al., 1998; Monteith, 1965).

$$\lambda \mathrm{ET} = \frac{\delta R^* + \rho_a C_p (e_s - e_a)/r_a}{\delta + \gamma(1 + r_s/r_a)} \tag{6}$$

In Equation 6, λ is the latent heat of vaporization (J/kg), ET is the evapotranspiration flux (kg/(m^2/s)), δ is the slope of the saturation vapor pressure–temperature relationship (Pa/K), R^* is net radiation minus the soil heat flux (W/m^2), ρ_a is the air density (kg/m^3), C_p is the specific heat of air (J/(kg/K)), $e_s - e_a$ is the vapor pressure deficit of the air (Pa), γ is the psychrometric constant (Pa/K), and r_s and r_a are the bulk surface resistance and aerodynamic resistance (s/m).

From Equation 6, the changes of ET (by unit temperature or derivative temperature change, the ET-T sensitivity) can be approximated (to the first order) by the sum of ET changes attributed to five variables: R^*, $e_s - e_a$, r_a, r_s, and δ in Equations 7–12 (Yang et al., 2019, with some errors fixed).

$$\Delta ET \approx \frac{\partial ET}{\partial R^*}\Delta R^* + \frac{\partial ET}{\partial (e_s - e_a)}\Delta(e_s - e_a) + \frac{\partial \mathrm{ET}}{\partial r_s}\Delta r_s + \frac{\partial ET}{\partial r_a}\Delta r_a + \frac{\partial ET}{\partial \delta}\Delta\delta \tag{7}$$

Where the five derivatives in the right-hand side of Equation 7 are respectively:

$$\frac{\partial ET}{\partial R^*} = \frac{\delta}{\lambda\left[\delta + \gamma\left(1 + \frac{r_s}{r_a}\right)\right]} \tag{8}$$

$$\frac{\partial ET}{\partial (e_s - e_a)} = \frac{\rho_a C_p}{\lambda r_a\left[\delta + \gamma\left(1 + \frac{r_s}{r_a}\right)\right]} \tag{9}$$

$$\frac{\partial ET}{\partial r_s} = \frac{-\gamma\left[\delta R^* + \frac{\rho_a C_p (e_s - e_a)}{r_a}\right]}{\lambda r_a\left[\delta + \gamma\left(1 + \frac{r_s}{r_a}\right)\right]^2} \tag{10}$$

$$\frac{\partial ET}{\partial r_a} = \frac{\gamma r_s\left[\delta R^* + \frac{\rho_a C_p (e_s - e_a)}{r_a}\right]}{\lambda {r_a}^2\left[\delta + \gamma\left(1 + \frac{r_s}{r_a}\right)\right]^2} - \frac{\rho_a C_p (e_s - e_a)}{\lambda {r_a}^2\left[\delta + \gamma\left(1 + \frac{r_s}{r_a}\right)\right]} \tag{11}$$

$$\frac{\partial ET}{\partial \delta} = \frac{R^*}{\lambda\left[\delta + \gamma\left(1 + \frac{r_s}{r_a}\right)\right]} - \frac{\delta R^* + \frac{\rho_a C_p (e_s - e_a)}{r_a}}{\lambda\left[\delta + \gamma\left(1 + \frac{r_s}{r_a}\right)\right]^2} \tag{12}$$

The variables δ, λ, γ, r_s, r_a, R^*, $e_s - e_a$, ρ_a are approximated as the averages between baseline and warming scenarios. A relatively small warming step is preferred to provide good approximations to the partial

derivatives. Therefore, we focus on 0.1°C warming when applying this method in the results section (however, we show results for 1°C and 3°C warming results in the supporting information as well). In our derivations, we used a 0.625 degree lat-long grid mesh to subsample the 1/16 degree lat-long study domain into 268 grid cells across the four basins. The subsampled mesh consisted of one 1/16-degree grid cell every 10 grid cell in each dimension (hence reducing the computational requirements for estimation of the partial derivatives in Equations 8–12 by a factor of 100). This subsampling is intended to capture the first-order variations of the hydroclimate factors reflected in Equations 8–12 across our study area. The r_s value is inverted from the Penman-Monteith equation along with other explicit model output variables. We used the VIC model in this analysis because (i) the VIC model should be representative of the other models in part because it generates the forcings (via the Bohn et al., 2013, algorithms) for the other models, and (ii) the VIC model has the variables required by Equations 8–12 above explicitly available as outputs.

4. Results

4.1. Multi-Model Streamflow Response to Seasonal Warming

Multi-model simulations of streamflow responses to seasonal warming using the four models are shown in Figure 1. In response to year-around warming, three out of four models (Catchment being the exception) show a reduction in annual streamflow in all four basins (Figure 1a), with reductions ranging from about 3% to about 19%. For the Catchment model, the annual runoff response to year-around warming is quite small, ranging from about a 3% reduction in the Colorado basin to about a 3% increase in the N. Sierra. Multi-model mean results show annual runoff declines of 7.5%, 5.6%, 2.0%, and 2.2% under 3°C warm season warming and 4.7%, 2.2%, 2.5%, and 3.2% under 3°C cool season warming, across the Colorado, Columbia, N. Sierra, and S. Sierra, respectively (Figures 1b and 1c, gray bars). The annual flow response to year-around warming is the net result of usually more substantial reductions in warm season streamflow and weaker increases in cool season streamflow.

Interestingly, warm season-only warming produces reductions in streamflow in the warm season and, to some extent, in the cool season for all four models and four basins. In contrast, cool season-only warming produces increased streamflow in the cool season and diminished streamflow in the warm season.

Figure 1 shows that for the Columbia Basin and Colorado basin, the annual streamflow decreases are mostly associated with warming in the warm season, but for the California basins, the decreases are more associated with cool season warming in VIC and SAC-SMA. Noah-MP shows slightly higher decreases under warm season warming than under cool season warming. The patterns in N. Sierra and S. Sierra from VIC are different from those in Das et al. (2011), which shows comparable decreases of streamflow under warm versus cool season warming. This difference arises from multiple sources: we used a higher resolution forcing and parameter (1/16 vs. 1/8 degrees lat-long), a newer version of VIC, and L13 forcings instead of Hamlet and Lettenmaier (hereafter H&L) forcing (Hamlet & Lettenmaier, 2005) for better consistency between forcing and parameters. We confirmed these sources of variation by setting up another experiment with estimated model version and parameters (the details of Das et al., 2011, model setup have been lost to time) with the same H&L 1/8 degree forcing in the same time range as Das et al. (2011). We then changed the 1/8 degree forcing to 1/16 degree to repeat the experiment. The 1/8 degree results in the N. Sierra and the S. Sierra show much more similar runoff response patterns as compared with Das et al. (2011), while the 1/16 degree results show a stronger response to cool season warming (Figure S3), suggesting a substantial resolution impact on the results. Nevertheless, we choose to present our results with the newer VIC version and higher spatial resolutions here for consistency with other models and potentially better representations of reality.

SAC-SMA performs differently than other models in the Colorado and Columbia basins, with a somewhat smaller annual streamflow decrease under warm season warming than under cool season warming. This different behavior is because SAC-SMA has a much smaller warm season ET increase compared with Noah-MP and VIC under warm season warming (Figures 2a, 2b, and 2d). As we will discuss later, warm season ET change dominates annual ET change under warm season warming. As a consequence, this smaller warm season ET yields a smaller annual ET increase, and thus a much smaller annual streamflow reduction under warm season warming than under cool season warming. We confirmed that the insensitivity of warm season ET to warm season warming in SAC-SMA is due to the constraining effect of the small increase of

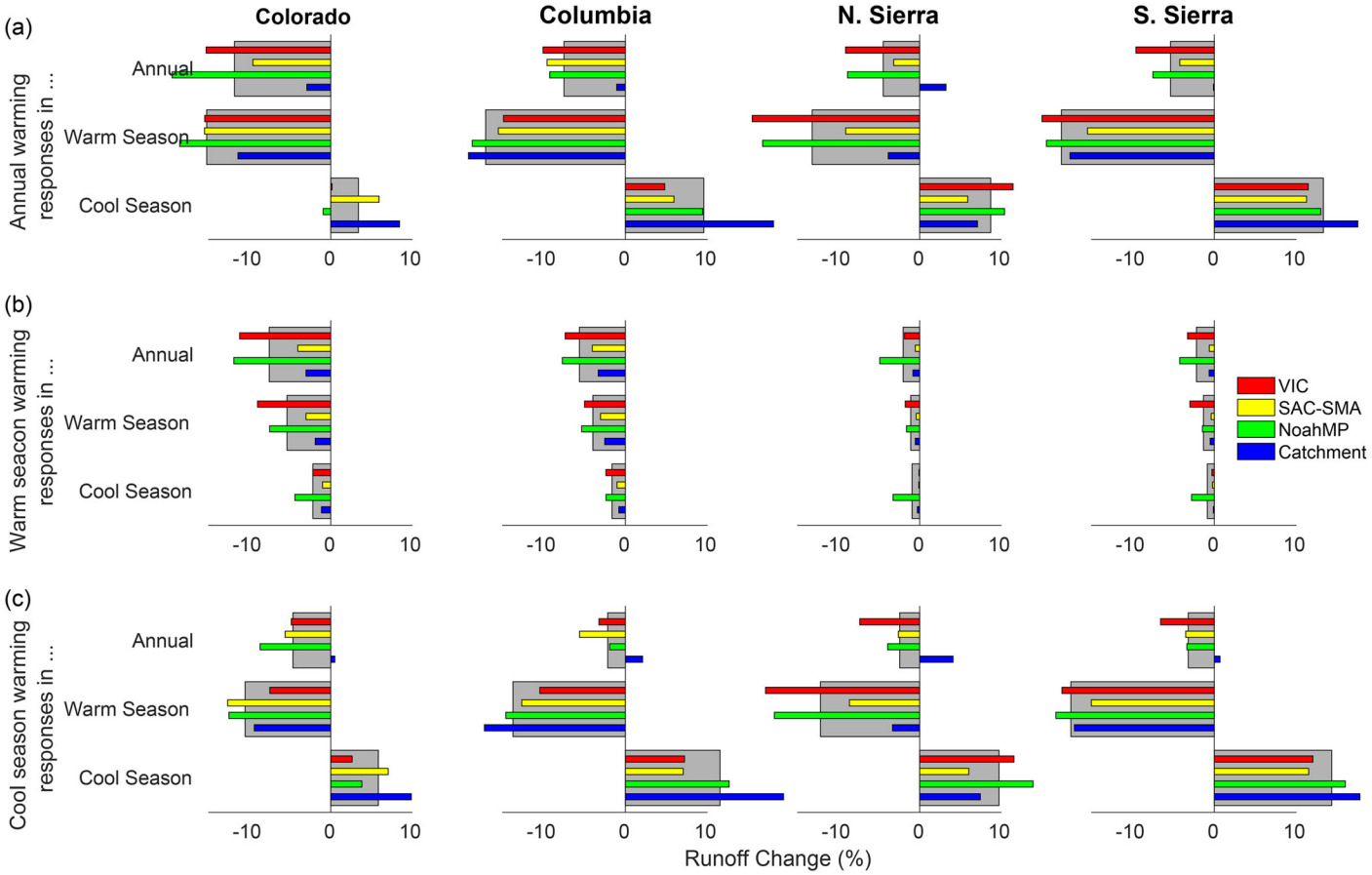

Figure 1. Multi-model streamflow changes in the annual, warm season (April to September) and cool season (October to March) averages, in response to (a) annual warming, (b) warm season warming, and (c) cool season warming scenarios. All values are percent changes relative to the average annual flow for the historical baseline run (1916–2018 water year), so the annual response equals the sum of warm and cool season responses. The gray bars show the multi-model mean responses, and the colored bars are each model's results.

PET (a forcing for SAC-SMA) under warm season warming. Unlike the other models, PET is not computed internally by the model and thus may not be well coupled with the variation of hydrological variables within SAC-SMA.

Figure 1 also shows that Catchment differs from the other models in its positive annual streamflow responses to cool season warming, which are negative for all the other models. This different behavior of Catchment arises from the model's abnormally quick snowmelt under cool season warming, especially in forested areas. We confirmed this argument by setting the vegetation parameter for forest pixels to short

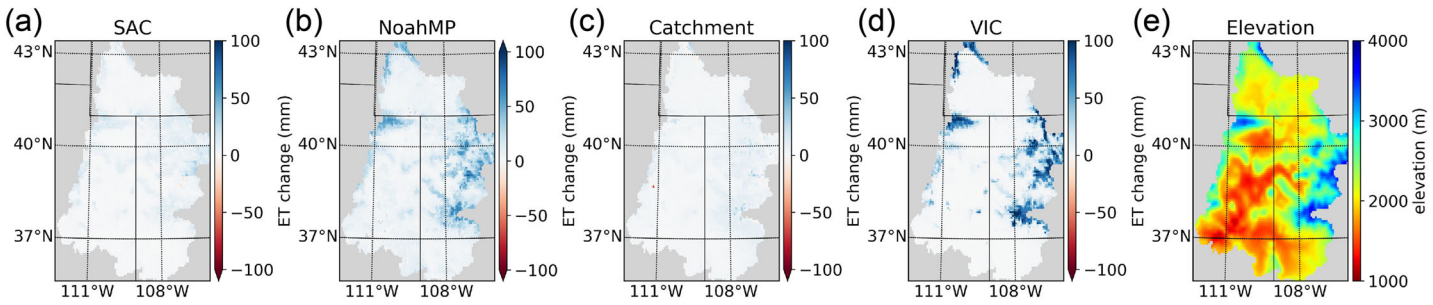

Figure 2. Multi-model 1916–2018 warm season average ET change under warm season warming, compared to the baseline run, using the Upper Colorado River basin as an example.

canopy, and the resulting annual streamflow responses under cool season warming change from positive to negative (Figure S4c), similar to the other models. This difference between higher and shorter canopies indicates an internal energy partitioning deficiency, including the lack of radiation attenuation and abnormally high ratio of sensible heat absorption during snowmelt, especially for tall canopies. We also confirmed the reason for the small warm season ET increase in Catchment (Figure 2c): under warm season warming, snow in the spring transition months (e.g., April) melts faster than in the baseline, leaving less soil moisture for the following warm months. This lack of soil moisture increases the fraction of not-saturated areas (less efficient in evapotranspiration). Also, it decreases the fraction of saturated areas (highly efficient in evapotranspiration) (Koster et al., 2000). These changes in area fraction largely offset the increase of evaporative demand within each of the area types under a warmer temperature and accumulate to a small warm season ET increase.

In the S. Sierra results, Catchment and Noah-MP show approximately neutral runoff responses under seasonal warming. In contrast, the SAC-SMA and VIC results show a significantly stronger annual runoff response under cool season warming. They are opposite to Das et al. (2011), in which S. Sierra's annual streamflow experienced similar decreases under both warm (3.6%) and cool (3.1%) season warming. This difference is not surprising given the large variation of the magnitude of asymmetry across models. As we cannot believe in any model more than the other ones, even the one used in Das et al. (2011), we focus on the multi-model mean (larger runoff response to cool season warming in the S. Sierra). In the other three basins, most of the models and multi-model mean show similar streamflow response patterns to Das et al. (2011), in which N. Sierra had slightly stronger decreases under cool season warming, and the Colorado and Columbia basins had larger annual streamflow decreases under warm season than under cool season warming. This spatially and temporally heterogeneous pattern across basins motivates questions as to the mechanisms that are responsible for the differences.

4.2. Comparison Between $Pref_{ET}$ and $Pref_{Q}$

Figure 3 confirms that $Pref_{ET}$ and $Pref_{Q}$ are nearly the same across basins with small differences between the two. The small differences are attributable to multiple causes that lead to the difference between P_a and $ET_a + Q_a$ in different warming scenarios: closure error of all four models within error limits; and SM and SWE differences between the beginning year and ending year. Nonetheless, such discrepancies between $Pref_{ET}$ and $Pref_{Q}$ are acceptable in the following discussions since they do not affect the relative order of the basins' response to seasonal warming (Figure 3). Therefore, in the interest of brevity, hereafter, we refer to $Pref_{ET}$, and everything is the same for $Pref_{Q}$.

Figure 3a shows that $Pref_{ET}$ is always positive except for in Catchment. For the other three models, Columbia and Colorado are always the basins with first and second largest $Pref_{ET}$, while the relative orders between the two basins with lower $Pref_{ET}$ (N. Sierra and S. Sierra) differ, which is probably within the uncertainty of model behaviors. Catchment's negative Pref values occur because its annual Q increases under cool season warming (see section 4.1). For example, for the Colorado basin, Catchment has $Pref_{Q}$ of around −6, meaning warm season warming causes annual Q to have six times larger response (decreasing) in the opposite direction to the response to cool season warming (increasing). This means that the annual Q decrease or ET loss in Catchment is only caused by warm season warming.

Across the models with positive $Pref_{ET}$, the relative order of the basins' $Pref_{ET}$ values is similar, while the magnitudes differ (Figure 3a). Although Catchment shows abnormally high runoff increases under cool season warming relative to the other three models, it is still a plausible outcome of cool season warming when more precipitation is partitioned into rainfall and less energy is available for evapotranspiration in winter, leading to higher runoff than in the baseline. To treat each model with equal weight and focus on the hydrological characteristics of the basins rather than model particulars, in the following sections, we focus on multi-model mean results across all four models.

4.3. Seasonal Factors Dominating the Annual ET Responses Under Seasonal Warming

Above, we have discussed the features of annual ET responses to seasonal warming. Here, we discuss the factors that contribute most to those features. We plot the seasonal and annual ET response to seasonal warming in Figure 4, to see whether one season dominates the annual ET change under the two seasonal warming scenarios.

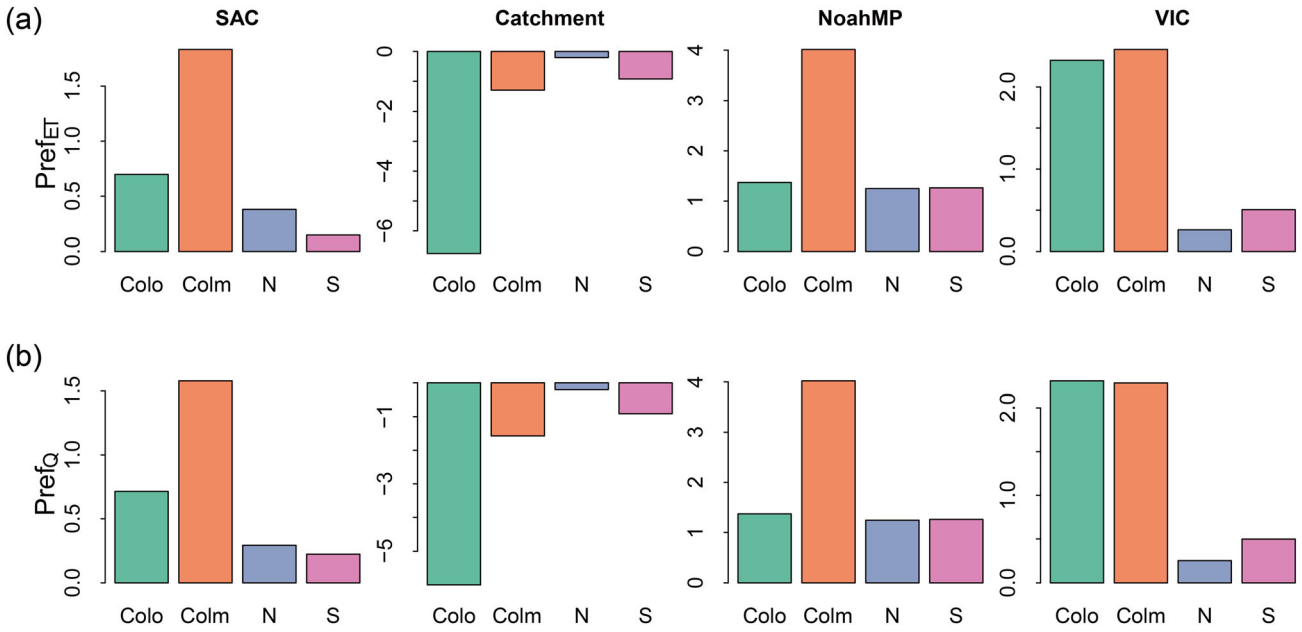

Figure 3. (a) $Pref_{ET}$ and (b) $Pref_{Q}$ across four basins estimated from outputs from the four models.

Figure 4 indicates the season contributing most to annual ET change for cool season and warm season warming. Our interpretation is as follows:

1. Under warm season warming, most of the ET increase occurs in the warm season, while the cool season ET increase is negligible (Figure 4a), which is also confirmed by monthly ET changes under warm season warming (Figures S5–S8, red lines). The negligible cool season ET (ET_c) change under warm season warming does not conflict with the simultaneous reduction in cool season streamflow (Figure 1b), because a greater portion of winter precipitation is used to satisfy a greater SM deficit at the end of the warm season, which significantly reduces runoff but not ET (Figures S5–S8, red lines). Therefore, the warm season ET change (ΔET_w) dominates the annual ET change.

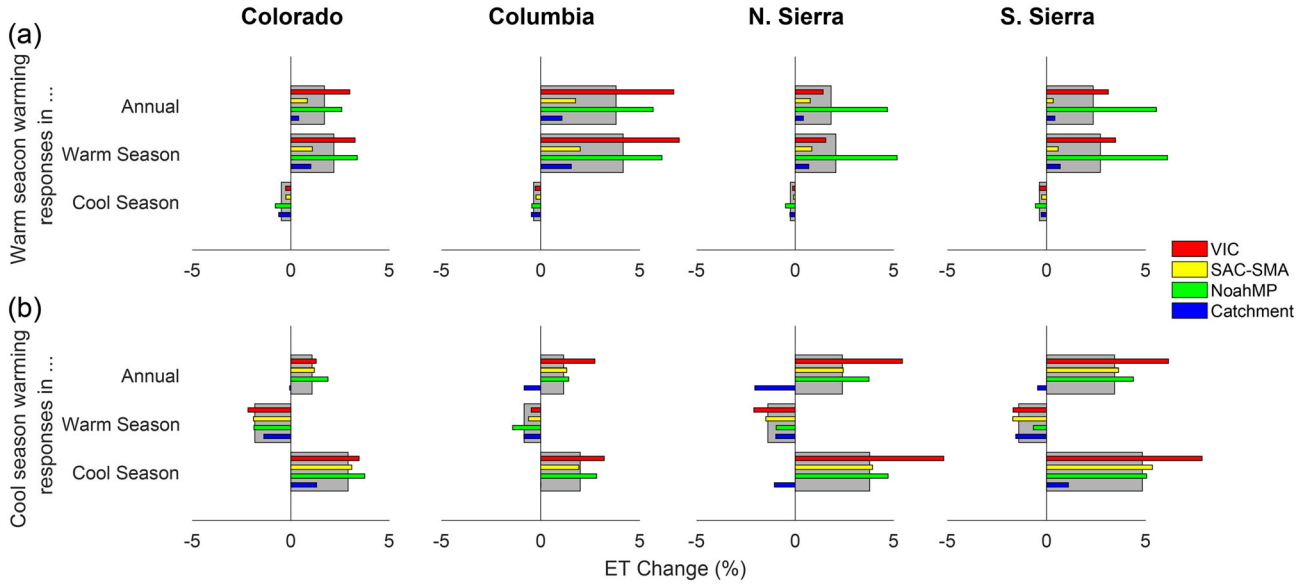

Figure 4. Multi-model ET changes in the annual, warm season (April to September) and cool season (October to March) averaged across 1916–2018 water year, in response to (a) warm season warming and (b) cool season warming. The layout is the same as in Figure 1, but for ET.

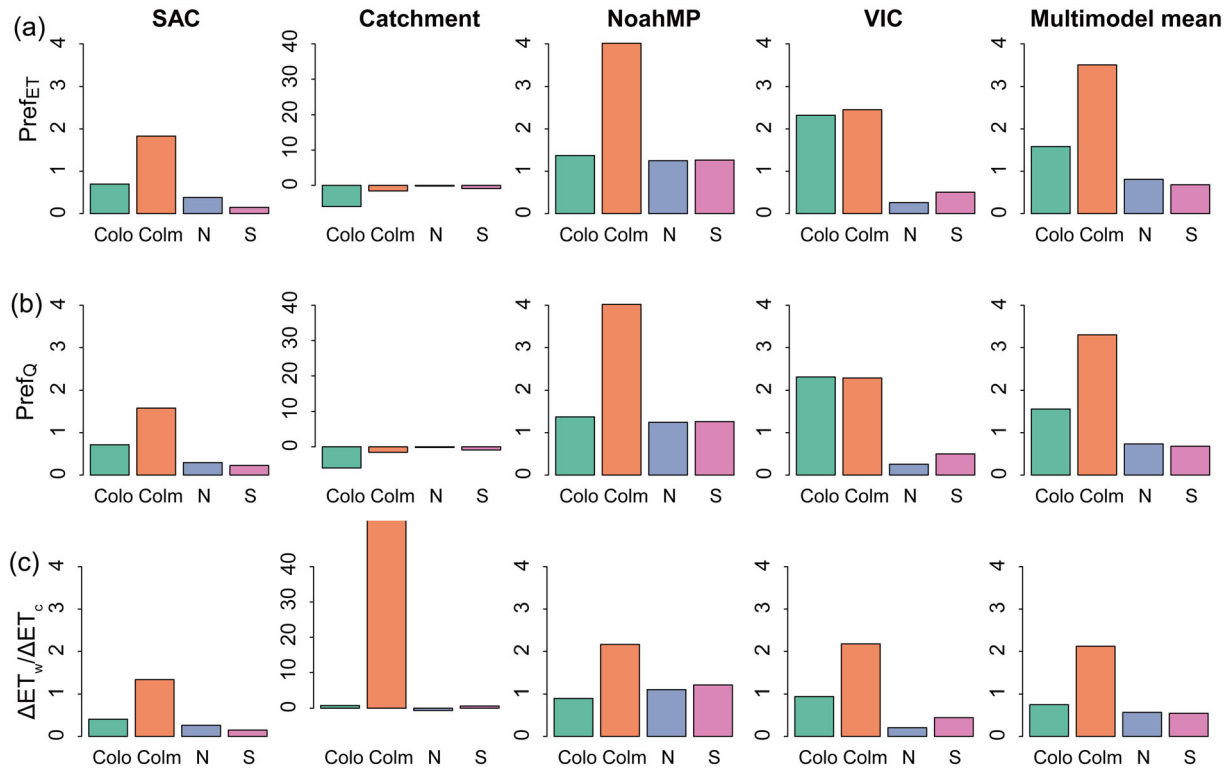

Figure 5. Bar plots of (a) Pref_{ET}, (b) Pref_{Q}, and (c) ET change ratio ($\frac{\Delta ET_w}{\Delta ET_c}$, also named as $\frac{\overline{\text{ET}_{\text{w, w3d}}} - \overline{\text{ET}_{\text{w, b}}}}{\overline{\text{ET}_{\text{c, c3d}}} - \overline{\text{ET}_{\text{c, b}}}}$ in Equation 5) across four basins for four models and the multi-model mean.

2. Under cool season warming, snowfall decreases as rainfall increases. Snowpack accumulation decreases while both runoff and snowmelt are accelerated. As a result, when the warm season comes, there is less accumulated snow than if there were no cool season warming. In this case, the annual ET is the result of two often opposing changes: ET_c change (usually increases) in warmer winters (Figure 4b, lowest bars), and ET_w decreases due to the increased evaporative resistance (a consequence of drier soils with less snowmelt supply in the summer) (Figure 4b, middle bars). Nevertheless, the increase in ET_c is usually much more substantial compared with the ET_w decrease (Figure 4b). Therefore, the cool season ET change (ΔET_c) dominates the annual ET change.

Considering both (a) and (b), we expect to see that the annual ET response to warm versus cool season warming is dominated by the ET changes within the warmed season. Therefore, the relative orders of Pref_{ET} and Pref_{Q} across basins should mostly follow the order of the ratio of ET_w change under warm season warming to ET_c change under cool season warming (Equation 5 in section 3.4). To check this, we plotted the Pref_{ET}, Pref_{Q}, and the ET change ratios across basins and models, as well as the multi-model mean in Figure 5.

The bar plots in Figure 5 confirm that the relative orders of Pref_{ET} and Pref_{Q} are highly consistent with the ET change ratio ($\frac{\Delta ET_w}{\Delta ET_c}$) on a multi-model mean basis, although the magnitudes differ (Figure 5, fifth column). We also further confirmed the consistency between the spatial pattern of Pref_{ET}, Pref_{Q}, and $\frac{\Delta ET_w}{\Delta ET_c}$ by plotting long-term climatological maps across four basins and four models (Figure S13).

4.4. Dominant Factors Controlling ET-Temperature Sensitivity in Warm and Cool Season

We confirmed in section 4.3 that $\frac{\Delta ET_w}{\Delta ET_c}$ dominates the Pref values. Now we attempt to determine whether changing water supply or evaporative demand is the main factor controlling $\frac{\Delta ET_w}{\Delta ET_c}$. Under only warm season warming with cool season temperature remaining unchanged, the moisture provided by the cool season

to the warm season (i.e., SM and SWE on 1 April) is nearly unchanged (Figures S9–S12, subplot a & b). Under only cool season warming with warm season temperature remaining unchanged, the moisture provided by the warm season to the cool season (i.e., mainly the SM on 1 October) is also nearly unchanged (Figures S9–S12, subplot e). Together with the fixed P_w and P_c, the ΔET_w and ΔET_c are mainly caused by the increasing evaporative demand associated with warmer temperatures in the warmed season, rather than water availability changes.

Given the two considerations discussed above, we investigate the pattern of ET-temperature (ET-T) sensitivity in this section, with a focus on the key factors that cause ET-T sensitivities to vary across basins. We start from four forcing variables that might strongly affect ET: vapor pressure deficit ($e_s - e_a$), air temperature (T_{air}), net radiation (R_{net}), and wind speed (u). Because snowmelt is also a dominant source of water for evapotranspiration in the warm season, we add a fifth term: gross incoming water (GIW). GIW for the cool season (GIW_c) is defined as the sum of soil moisture (SM) and snow water storage (SWE) at the beginning of the cool season (defined as 1 October) plus the cool season precipitation. GIW for the warm season (GIW_w) is defined as the sum of soil moisture (SM) and snow water storage (SWE) at the beginning of the warm season (defined as 1 April) plus the warm season precipitation. In Figure 6, we show the relationship between multi-model mean ET-T sensitivity and each of the five variables on a basin-averaged, annual basis. Each dot denotes the outputs of a single year out of 1916 to 2018. The red dots in Figure 6 represent the warm season ET-T sensitivity together with each of the five variables under warm season warming, and the blue dots are for cool season warming. We evaluate correlations based on normalized values of the variables using the Pearson correlation method, and linear regressions are fit to the points. The correlation and the *p*-value of the correlations are in the legends (Figures 6a–6e), where $p = 5\%$ is the significance level.

For $e_s - e_a$ (Figure 6a), the correlation values in the warm season are all negative and significant. The correlation values in the cool season are all negative, and only two of them are significant. The warm season has larger correlations, and the slopes of dET/dT versus $e_s - e_a$ linear regression lines are generally higher as compared with that of the cool season. These patterns indicate that decreasing $e_s - e_a$ is associated with increasing ET-T sensitivity in the warm season, while the cool season $e_s - e_a$ does not have a strong relationship with the ET-T sensitivity.

For T_{air} (Figure 6b), the correlation values in the warm season are all negative and significant. The correlation values in the cool season are mostly significant, and the significant ones are all positive. The slopes of dET/dT versus T_{air} linear regression lines are higher for the warm season than for the cool season. These patterns indicate that strong ET-T sensitivities are associated with decreases in the warm season T_{air} and increases in the cool season T_{air}.

For R_{net} (Figure 6c), the correlations in the warm season are all negative and significant, which may well be reflecting the relationship between the decreasing ET-T sensitivity and stronger warm season T_{air} (usually with higher R_{net}). In the cool season, the significant correlations (for dET/dT vs. R_{net}) shift from negative (Colorado) to positive (Columbia and N. Sierra), not consistent across basins, suggesting that the other variables' yearly change may influence the relationship between R_{net} and ET-T sensitivity.

For GIW (Figure 6d), correlation values in both seasons are positive. In the warm season, all basins' correlations are significant; in the cool season, the correlation in the Colorado and Columbia basins are significant. Therefore, despite GIW insubstantially differs between warmed season and baseline, thus is not the main cause of ET change, it still regulates ET-T sensitivity. For wind speed (Figure 6e), few of the correlations are significant. Therefore, we ignore the effect of wind speed on ET-T sensitivity in our subsequent discussion.

Considering all the above, we summarize as follows: ET-T sensitivity generally increases with GIW, and this tendency is stronger when T_{air} is high (slopes are higher for the warm season than for the cool season; Figure 6d). When T_{air} is low (in the cool season), ET-T sensitivities increase with T_{air}. When T_{air} is high (in the warm season), ET-T sensitivity decreases with T_{air}, $e_s - e_a$, and R_{net}. Since $e_s - e_a$ and T_{air} are highly correlated (Figure S14), and T_{air} usually increases with R_{net} in the warm season, the relationship can be simplified to be that ET-T sensitivity decreases with T_{air} in the warm season. Wind speed has no substantial relationship with ET-T sensitivity in either season. These patterns identified from yearly data within each basin

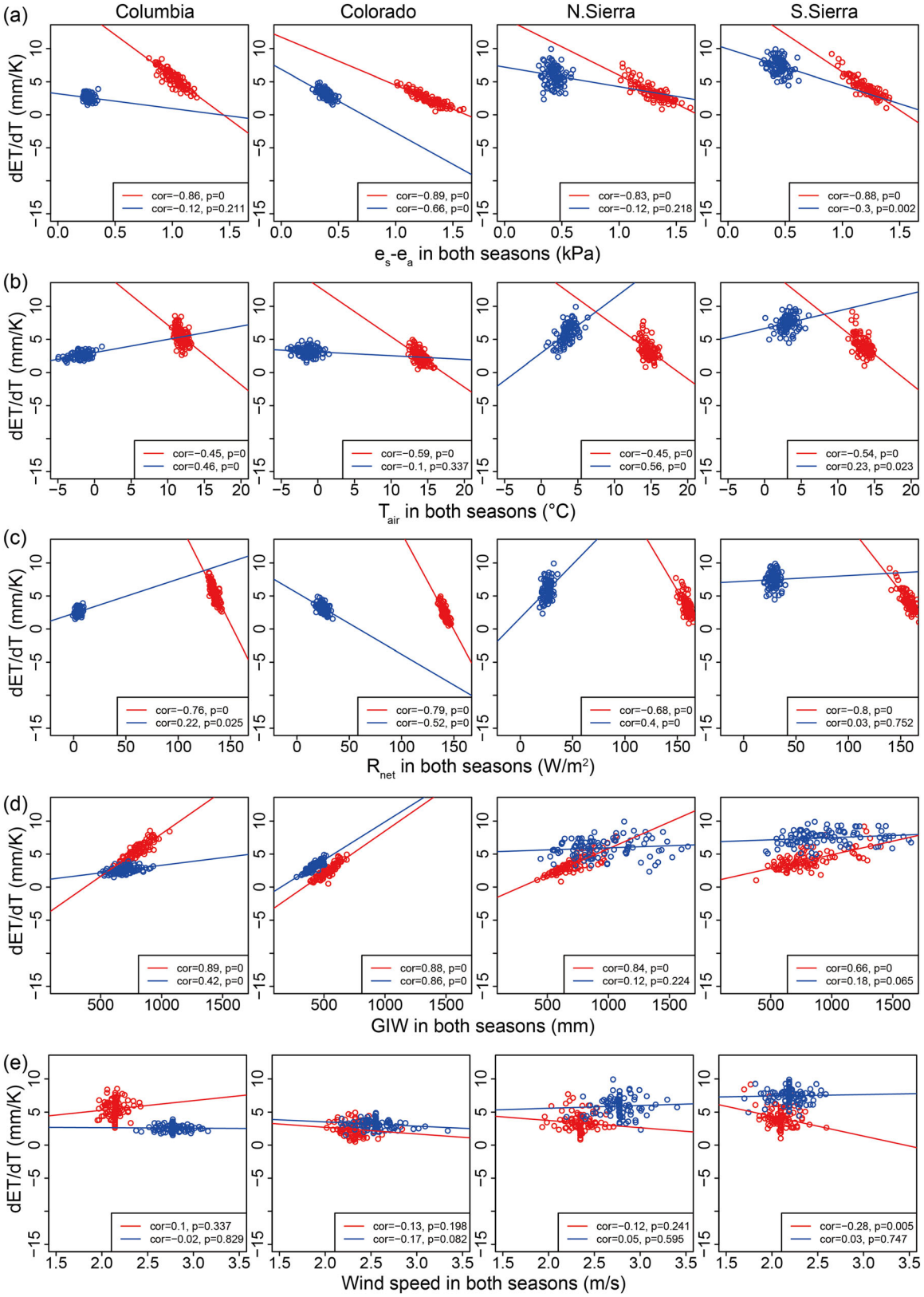

Figure 6. Scatterplots of the relationship between ET-T sensitivity and (a) $e_s - e_a$, (b) T_{air}, (c) R_{net}, (d) GIW, and (e) wind speed. dET/dT, GIW, and R_{net} are from the multi-model mean. The other variables are from forcings shared by the four models.

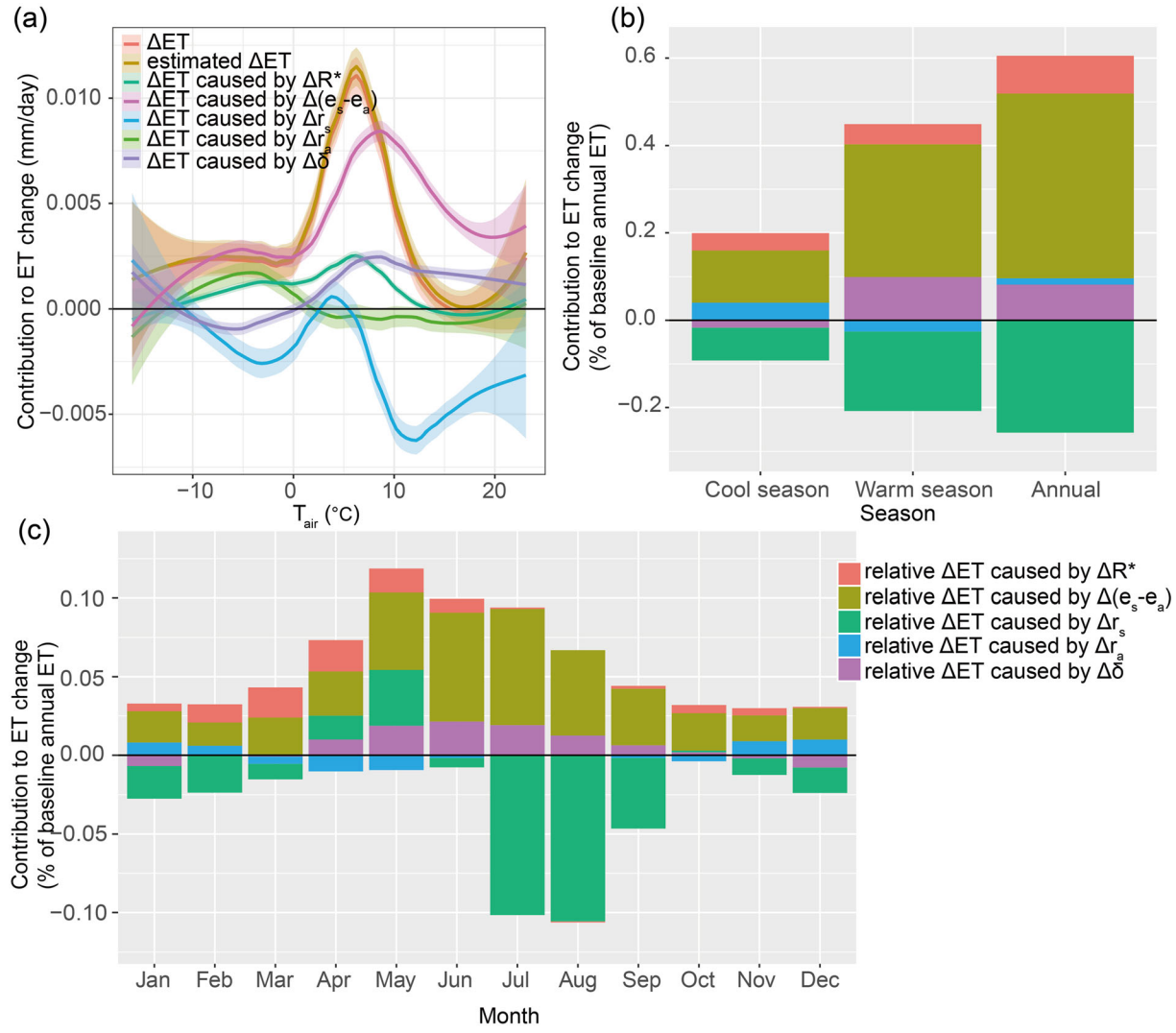

Figure 7. Attribution of R^*, $e_s - e_a$, r_a, r_s, and δ to warming-induced ET change. (a) LOWESS-smoothed contribution of the five factors to ET change at different temperatures under 0.1°C seasonal warming (cool season and warm season data merged). (b) Seasonal and annual contributions of the factors to ET change (relative to baseline annual ET) under 0.1°C annual warming. (c) Monthly contributions of the factors to ET change (relative to baseline annual ET) under 0.1°C annual warming. The smooth span parameter in (a) is 0.5, and the shadows in (a) indicate the confidence interval (level = 0.95).

are confirmed across different basins (Figure S15) and are also supported by pixel-by-pixel scatterplots across all four basins (Figure S16).

4.5. Understanding the Relationship Between T_{air} and ET-T Sensitivity

In the previous section, we confirmed that T_{air} and water availability (GIW) are dominating ET-T sensitivity. It is easy to understand that in general, when energy does not limit evapotranspiration, higher water availability favors higher seasonal ET-T sensitivity. What remains to understand is, what causes the shift from positive dET/dT versus T relationships to negative when T_{air} increases from cool to warm? With Equations 7–12, we illustrate the contribution of the five variable's associated ET change to the total ET change at different temperatures across the cool and the warm season (Figure 7a) and contribution cumulated across-temperature at monthly (Figure 7c), seasonal and annual scale (Figure 7b) based on a set of subsampled pixels (0.625 lat-long deg resolution grid mesh over 1/16 lat-long deg) using the VIC model.

Figure 7a shows that ET change caused by $e_s - e_a$ is the largest positive contributor to the Δ*ET* pattern across different temperatures, followed by R^* and δ, and r_a is the least influential. Unlike the other four factors, the

effect of r_s is mostly negative and has a comparable canceling effect on the contribution from $e_s - e_a$. Nonetheless, all five factors support the observed positive-to-negative shift of the dET/dT versus T_{air} relationship.

The variations of the five contributors with T_{air} arise from different reasons. The variation of $\frac{\partial ET}{\partial(e_s - e_a)}\Delta(e_s - e_a)$ with T_{air} is an effect of both the enhanced rate of increasing atmospheric water vapor holding capacity (thus larger $\Delta(e_s - e_a)$ and $\Delta\delta$, Figures S17e and S17n) and the larger r_s driven by elevated $e_s - e_a$ (thus smaller $\frac{\partial ET}{\partial(e_s - e_a)}$, Equation 9, Figure S17d) under a warmer temperature. The variation of $\frac{\partial ET}{\partial R^*}\Delta R^*$ with T_{air} is due to the higher r_s and smaller r_a at a higher temperature (thus decreasing $\frac{\partial ET}{\partial R^*}$, Equation 8, Figure S17a), together with the snowmelt-albedo feedback (Milly & Dunne, 2020) that max out ΔR^* when snowpack shrinks most rapidly (Figure S17b). The variation of $\frac{\partial ET}{\partial \delta}\Delta\delta$ with T_{air} is mainly due to the competing effect of increasing R* (and r_s/r_a) that could increase (or decrease) the first right-hand term (dominant term) of Equation 12 as temperature increases. The variation of $\frac{\partial ET}{\partial r_a}\Delta r_a$ with T_{air} is an effect of both stronger ET to r_a sensitivity (Equation 11, Figure S17j) and weaker r_a to temperature sensitivity at warmer temperatures (Figure S17k). The opposite contribution from r_s and $e_s - e_a$ to ΔET is closely related to the r_s increase in response to the elevated $(e_s - e_a)$ as temperature increases.

The rank of the five factors' contribution in Figure 7a mostly persists in Figure 7b at annual scale ($e_s - e_a$: 0.423%, R*: 0.086%, δ: 0.082%, r_s: −0.257%, and r_a: 0.014%) and seasonal scale. In the warm season, R* shows less contribution (0.046%) than δ (0.099%) to the warm season ET change, which follows the lower curve of R* than δ when T_{air} is above around 7°C in Figure 7a. In the cool season, both R* (0.040%) and r_a (0.040%) play a more significant role than δ (−0.017%) in their contribution to cool season ET change (Figure 7b).

The monthly scale contribution in Figure 7c shows a larger R* contribution from March to April, which is supported by the larger changes of R_{net} during snowmelt season due to the albedo contrast between snow cover and snow-free surfaces under warming (Milly & Dunne, 2020). $e_s - e_a$ and δ show larger contributions in the warm season, especially the early summer, which is supported by their variation patterns in Figure 7a. r_s continue to cancel out effects of $e_s - e_a$.

Combining Figures 7a–7c, the increasing trend of dET/dT versus T relationship is primarily driven by the enhanced rate of water holding capacity (thus the larger $\Delta(e_s - e_a)$ and $\Delta\delta$), and the snowmelt-albedo feedback (thus the larger ΔR^*). The decreasing trend of dET/dT versus T relationship is primarily driven by the decreasing snowmelt-albedo feedback (thus the smaller ΔR^*), larger r_s, and smaller r_a over warmer (less stable) surfaces (thus the smaller $\frac{\partial ET}{\partial(e_s - e_a)}$, $\frac{\partial ET}{\partial R^*}$, and $\frac{\partial ET}{\partial \delta}$). We repeated the analysis with 1°C and 3°C warming, and the patterns are similar to 0.1°C warming (Figures S18a–S18c and S19a–S19c), indicating that our findings are robust under different warming magnitudes at least within 3°C.

Above, we explained the variation patterns of dET/dT with temperature. This variation explains the differences in $\Delta ET_w/\Delta ET_c$, thus differences in Pref values across basins with different temperatures. Because ET-T sensitivity increases with temperature in cool environments, ΔET_c is higher in basins with relatively warm cool seasons. Similarly, the ET-T sensitivity decreases with temperature in warm environments, so ΔET_w is lower in basins with relatively warm warm seasons. In other words, warmer basins have smaller ΔET_w and larger ΔET_c, thus smaller $\Delta ET_w/\Delta ET_c$, and thus have smaller $Pref_{ET}$ and $Pref_Q$ values than other basins. Similarly, the positive relationship between GIW and dET/dT indicates that basins with a larger warm versus cool season GIW ratio will have larger $\Delta ET_w/\Delta ET_c$ and larger Pref values, other factors being equal.

5. Discussion

We recognize that real-world warming is not just adding a constant and usually involves changes in mean, variance, and even distribution. However, this uncertainty of warming pattern emphasizes the importance

of sensitivity analysis since it captures the unchanged out of change. One challenge water managers face is that every 5 years or so, a new set of IPCC predictions comes out. Inevitably they are not entirely consistent. One typical example is the Das et al. (2011) warm/cool season warming projections for CMIP3 as contrasted with the ones we show for CMIP5 (Figure S2). The multi-model work we performed here generated sensitivity estimates that are neither dependent on a specific set of warming predictions nor a specific model, provided a detailed explanation of the basins' seasonally dependent sensitivities, and unrevealed the key sub-annual processes that govern annual runoff reduction. Our work is beneficial to adaptive water management under an asymmetrical warming future.

We discovered that the variation of ET-T sensitivity is mainly a function of air temperature. The basins with warmer T_{air} generally have higher (lower) ET-T sensitivity in the cool (warm) season, thus smaller Pref values than the other basins. However, the ΔR^* is less directly related to T_{air} than the other four variables ($e_s - e_a$, r_s, r_a, and δ). The snowmelt-radiation effect used to explain ΔR^* variation with T_{air} has only been documented in the Colorado basin in Milly and Dunne (2020). Here we added an investigation of the processes connecting ΔR^* and T_{air} in the snowmelt-albedo feedback across the four basins using the VIC model. We found that the ΔR^* change is mainly due to upward shortwave change that mostly occurs from late fall through spring (Figures S20c and S20d), which is consistent with the decrease of effective albedo due to the transition from snow cover to snow-free conditions in a warmer climate. We further derived the relationships among the factors affecting the change of albedo and upward shortwave between the baseline and warming scenarios:

$$\Delta\alpha_{ttl} = \Delta f_s(\alpha_s - \alpha_{non-s}) + f_s'\Delta\alpha_s + \left(1 - f_s'\right)\Delta\alpha_{non-s} \tag{13}$$

$$\Delta SW_{up} = SW_{down}{}^*\Delta\alpha_{ttl} \tag{14}$$

where Δ is the baseline value minus the warmer climate value; α_{ttl} is the basin-average albedo, considering both snow-covered and snow-free regions; α_s is snow albedo, α_{non-s} is non-snow region albedo; f_s is baseline snow cover fraction (as a ratio of basin area); and f_s' is snow cover fraction under warmed scenarios (derivation of Equation 13 is shown in Text S3). Based on Equations 13 and 14, our interpretations are as follows.

In the cool season, the variation of snow cover fraction (Δf_s) depends on several main factors. First, basins with thinner snow and warmer temperatures would generally have a larger fractional Δf_s (i.e., $\Delta f_s/f_s$) (Figure S21a); for basins with similar $\Delta f_s/f_s$, a larger baseline snow cover fraction (f_s) would yield a larger Δf_s (e.g., Colorado and Columbia vs. S. Sierra, Figure S21a). Second, for basins with similar Δf_s, smaller α_{non-s} (usually means less grass and more trees) generally leads to larger albedo changes ($\Delta\alpha_{ttl}$) (Figure S22a), and a smaller f_s' between basins with similar α_{non-s} would yield a larger $\Delta\alpha_{ttl}$ (e.g., the S. Sierra and Columbia, Figure S22a). Third, for basins with similar albedo changes, a stronger downward shortwave would yield a stronger upward shortwave change (Equation 14), thus larger ΔR^*. All of these features that lead to a stronger cool season ΔR^* (larger Δf_s, smaller α_{non-s}, and stronger downward shortwave) are more prone to occur in basins with warmer temperatures, explaining the smaller ΔR^* at lower T_{air} in the cool environment/season (Figure S17b).

In the warm season, similar factors are functioning but Δf_s becomes the most influential factor of ΔR^*. Initially, a larger fraction of snow cover remains in basins of a cooler temperature, which allows greater snow cover reductions per temperature increment across the warm season (Figure S21b), leading to more SW absorption under similar downward shortwave, and consequently larger ΔR^*. These processes explain the larger ΔR^* at lower T_{air} in the warm environment/season (Figure S17b). The factors considered above presumably have a dominant contribution to the variation of ΔR^* because residual factors ($\Delta\alpha_s$ and $\Delta\alpha_{non-s}$) have relatively minor variations (e.g., α_s is constantly at 0.85 in VIC results). The influence of these residual factors is beyond the scope of this study, but studies that consider the albedo change of snowpack and land cover are needed in the future.

Our findings relative to the five variables' contribution to annual ET change generally agree with Yang et al. (2019), with the slight difference that our results show a larger contribution from δ. Yang et al. (2019) argued that elevated $[CO_2]$ is the primary reason for the r_s increase and the canceling effect between vapor

pressure deficit-driven and r_s-driven ET change. They base this statement on comparison of CMIP5 projections with models that do not consider either the $[CO_2]$ impact or vapor pressure deficit impact on r_s and attribute the difference primarily to the lack of representation of $[CO_2]$ impact. However, the canceling pattern persists in our offline model (VIC) that only considers the vapor pressure deficit impact on r_s, suggesting a less dominant contribution from $[CO_2]$ to r_s increase and dET/dT than predicted by Yang et al. (2019). It should be noted that the feedback of elevated humidity from enhanced ET on $e_s - e_a$ is not considered in our land surface modeling, so the increase of $e_s - e_a$ resulting from warming is likely overestimated, which might explain our larger $e_s - e_a$ contribution to dET/dT as compared to Milly and Dunne (2020).

We note that there are some limitations on our approximations of Pref using $\Delta ET_w/\Delta ET_c$ (Equation 5). Under cool season warming, ET_w decrease compensates ET_c increase and causes annual ET increase to be smaller than ET_c increase. This compensation effect causes Pref to be larger than $\Delta ET_w/\Delta ET_c$. Therefore, our conclusion is conservative as to the relative importance of warm season warming on annual runoff response, especially in arid/semi-arid basins like the Colorado basin, where low runoff efficiency causes snowmelt reduction to primarily show in ET_w reduction.

We follow the definition of warm and cool season division in Das et al. (2011) because one of the main points of this paper is to explain why the observed runoff response in that paper occurred. However, we note that the snowmelt season may be more sensitive to temperature and can cross our season division. Hence we test the robustness of our conclusion by revising the definition of the warm season and cool season to ensure that the snowmelt season is reliably spanned by the warm season. We did an analysis and found the dates of basin-average peak SWE are mostly in March (Colorado: 12 March; Columbia: 25 March; N. Sierra: 27 February; S. Sierra: 20 March), so we shifted the warm season to be March to September, and the cool season to be October to February. For the most part, the differences between the results from shifted seasons and original season division are insubstantial (Figure S23 vs. S24). We also tested the influence of warming magnitude by conducting an additional test with 1°C warming. The results show similar Pref values (Table S3) and a similar pattern of runoff response to temperature warming (around one third in response magnitude than 3°C warming, Figure S23 vs. S25), suggesting that different levels of warming asymmetry (at least within 3°C) would not alter our analysis and conclusions. We also verified the robustness of runoff response patterns against precipitation change by perturbing the precipitation forcing with CMIP5 projected precipitation changes (Figure S23 vs. S26). These three experiments suggest that our conclusion holds under potentially changing conditions.

Das et al. (2011) suggest that extra liquid water input (LWI: the sum of rainfall and snowmelt) during winter offsets the water reduction in the warm season and decreases the annual runoff reduction under year-round warming. The roles of extra rainfall, extra snowmelt, and extra warm season evaporative demand are intertwined together in their discussion. Here we did an investigation to separate the impact of the fraction of rainfall on runoff by modifying the four models' precipitation partition scheme to increase the fraction of rainfall and leave temperature unperturbed. We found that the warmer basins do not necessarily have a larger annual rainfall ratio increase, and the rainfall ratio increase does not make much difference (decrease) of annual Q in the four basins (Tables S4–S7). This limited impact of rainfall ratio on annual streamflow change is because either warming or the model option that changes precipitation partition is only affecting the rainfall-snowfall transition zone (arguably a small part of a basin).

The four models captured the observed runoff seasonality across the four basins (Figure S1). More important than the models' calibration to historical observations is their ability to reproduce inferred sensitivities from the historical record. Consistent with the argument for sensitivity evaluations, we checked the model performance in reproducing PET-elasticity ($\boldsymbol{\varepsilon_{PET}}$) and P-elasticity ($\boldsymbol{\varepsilon_P}$) using a nonparametric estimator and Dooge's complementary relationship (Dooge, 1992; Sankarasubramanian et al., 2001). Models generally yield more positive $\boldsymbol{\varepsilon_P}$ and more negative $\boldsymbol{\varepsilon_{PET}}$ than the observations (Tables S8 and S9), consistent with the findings in Vano et al. (2012). The difference across modeled and observed $\boldsymbol{\varepsilon}$ values are not surprising, possibly because the climate variables are less controllable in observations and a Budyko-like relationship is not embedded in the nonparametric estimator (Xiao et al., 2020). Given the large variations of $\boldsymbol{\varepsilon}$ values in literature (Vano et al., 2012; Xiao et al., 2020), our modeled and observation-based $\boldsymbol{\varepsilon_P}$ shows a reasonable degree of similarity (Tables S8 and S9).

6. Conclusions

We conducted a multi-model simulation of streamflow response to warm and cool season warming across four regionally important basins in the Western United States, evaluated the consistency among models in their streamflow response predictions, and explored the key processes governing the basins' seasonally dependent runoff sensitivities. We conclude that

1. The response patterns of (e.g., annual) runoff to cold versus warm season warming is generally consistent across models. Moreover, our multi-model averages are overall consistent with the results of Das et al. (2011) for the single model (VIC) used in that study. Compared with the impact of cool season warming, warm season warming always has the largest relative impact on annual streamflow change in the Columbia Basin. This signature becomes progressively less for the Colorado basin and is smaller still for the N. Sierra and S. Sierra basins.
2. The ratio of ET-T sensitivity in warm versus cool season warming constrains the relative rank (across basins) of streamflow response asymmetry to warm versus cool season warming. The ET-T sensitivity is closely associated with the basins' water availability (GIW) and T_{air}. The ET-T sensitivity generally increases with water availability, and this tendency is strongest when T_{air} is high. When T_{air} is low, the ET-T sensitivity mainly increases with T_{air}, whereas when T_{air} is high, the ET-T sensitivity decreases with T_{air}.
3. The increasing trend of dET/dT versus T_{air} in the cool months is primarily driven by the enhanced rate of water holding capacity and a stronger snowmelt-albedo feedback. The decreasing trend of dET/dT versus T_{air} is primarily driven by increased r_s and decreased r_a, and a weaker snowmelt-albedo feedback due to less remaining snowpack in warmer basins. The positive annual ET-T sensitivity is contributed mostly by the vapor pressure deficit, followed by available radiation, and slope of the saturated vapor pressure curve, with r_a the smallest (positive) contributor and r_s contributing negatively.
4. The pattern of ET-T sensitivity indicates that basins with colder winters and cooler summers, and higher warm season versus cool season GIW ratios (e.g., the Columbia Basin and the Colorado basin), have a stronger response to warm season warming than to cool season warming. Cool basins tend to have a larger annual runoff response to warm season relative to cool season warming.

Acknowledgments

We acknowledge the World Climate Research Programme's Working Group on Coupled Modeling, which is responsible for the Climate Model Intercomparison Project (CMIP) and its archive, and we thank the climate modeling groups (listed in Table S1) for producing and making available their model output. The U.S. Department of Energy's Program for Climate Model Diagnosis and Intercomparison provides coordinating support for CMIP and led development of software infrastructure in partnership with the Global Organization for Earth System Science Portals. We acknowledge the Downscaled CMIP3 and CMIP5 Climate and Hydrology Projections archive online (https://gdo-dcp.ucllnl.org/downscaled_cmip_projections/). Funding for this work was provided in part by the NOAA Regional Integrated Sciences and Assessments (RISA) program via support to the California Nevada Climate Applications Program (CNAP) at the Scripps Institution of Oceanography, grant number NA17OAR4310284, under sub-award to the University of California, Los Angeles. We acknowledge Kimberly Wang of UCLA's Land Surface Hydrology Research Group for help in proofreading.

Data Availability Statement

Data and codes used in our paper are publicly accessible at the following URLs: L13 forcings 1915–2011 (ftp://livnehpublicstorage.colorado.edu/public/Livneh.2013.CONUS.Dataset/Meteorology.asc.v.1.2.1915.2011.bz2/), and 2012–2018, extended by Lu Su at UCLA's Land Surface Hydrology Research Group (ftp://livnehpublicstorage.colorado.edu/public/sulu). VIC-4.1.2g (https://github.com/UW-Hydro/VIC/releases/tag/VIC.4.1.2.g), Noah-MP hrldas version 3.9 (https://github.com/NCAR/hrldas-release/tree/master/HRLDAS), Catchment are available as a part of the GEOS source code under the NASA Open-Source agreement (http://opensource.gsfc.nasa.gov/projects/GEOS-5). SAC-SMA can be obtained by emailing dist_hydro_mod@infolist.nws.noaa.gov or nws.nwc.ops@noaa.gov, and the code will be available through FTP to the requestor. Other representative data related to our results are available online (https://doi.org/10.6084/m9.figshare.11605818.v3).

References

Allen, R. G., Pereira, L. S., Raes, D., & Smith, M. (1998). FAO irrigation and drainage paper no. 56. *Rome: Food and Agriculture Organization of the United Nations*, *56*(97), e156.

Bay-Delta Office, California Department of Water Resources. (2007). *California Central Valley unimpaired flow data fourth edition draft*. California: Bay-Delta Office, California Department of Water Resources. Retrieved from https://www.waterboards.ca.gov/waterrights/water_issues/programs/bay_delta/bay_delta_plan/water_quality_control_planning/docs/sjrf_spprtinfo/dwr_2007a.pdf

Bohn, T. J., Livneh, B., Oyler, J. W., Running, S. W., Nijssen, B., & Lettenmaier, D. P. (2013). Global evaluation of MTCLIM and related algorithms for forcing of ecological and hydrological models. *Agricultural and Forest Meteorology*, *176*, 38–49. https://doi.org/10.1016/j.agrformet.2013.03.003

Bonneville Power Administration. (2019). https://www.bpa.gov/p/Power-Products/Historical-Streamflow-Data/Pages/No-Regulation-No-Irrigation-Data.aspx

Burnash, R. J., Ferral, R. L., & McGuire, R. A. (1973). *A generalized streamflow simulation system: Conceptual modeling for digital computers*. Sacramento: US Department of Commerce, National Weather Service, and State of California, Department of Water Resources.

California Data exchange center. (2018). http://cdec.water.ca.gov/dynamicapp/QueryWY

California Department of Water Resources, Climate Change Technical Advisory Group. (2015). In E. Lynn, A. Schwarz, J. Anderson, M. Correa (Eds.), *Perspectives and guidance for climate change analysis* (pp. 1–140). Sacramento, CA: DWR Division of Statewide

Integrated Water Management (DSIWM). Retrieved from https://water.ca.gov/LegacyFiles/climatechange/docs/2015/Perspectives_Guidance_Climate_Change_Analysis.pdf

Das, T., Pierce, D. W., Cayan, D. R., Vano, J. A., & Lettenmaier, D. P. (2011). The importance of warm season warming to western US streamflow changes. *Geophysical Research Letters*, *38*, L23403. https://doi.org/10.1029/2011GL049660

Dooge, J. C. I. (1992). Sensitivity of runoff to climate change: A Hortonian approach. *Bulletin of the American Meteorological Society*, *73*. https://doi.org/10.1175/1520-0477(1992)073<2013:sortcc>2.0.co;2

Gergel, D. R., Nijssen, B., Abatzoglou, J. T., Lettenmaier, D. P., & Stumbaugh, M. R. (2017). Effects of climate change on snowpack and fire potential in the western USA. *Climatic Change*, *141*(2), 287–299. https://doi.org/10.1007/s10584-017-1899-y

Hamlet, A. F., & Lettenmaier, D. P. (2005). Production of temporally consistent gridded precipitation and temperature fields for the continental United States. *Journal of Hydrometeorology*, *6*(3), 330–336. https://doi.org/10.1175/jhm420.1

Hamlet, A. F., Mote, P. W., Clark, M. P., & Lettenmaier, D. P. (2005). Effects of temperature and precipitation variability on snowpack trends in the western United States. *Journal of Climate*, *18*(21), 4545–4561. https://doi.org/10.1175/JCLI3538.1

Hayhoe, K., Cayan, D., Field, C. B., Frumhoff, P. C., Maurer, E. P., Miller, N. L., et al. (2004). Emissions pathways, climate change and impacts on California. *Proceedings of the National Academy of Sciences*, *101*(34), 12,422–12,427. https://doi.org/10.1073/pnas.0404500101

Kalnay, E., Kanamitsu, M., Kistler, R., Collins, W., Deaven, D., Gandin, L., et al. (1996). The NCEP/NCAR 40-year reanalysis project. *Bulletin of the American Meteorological Society*, *77*(3), 437–472. https://doi.org/10.1175/1520-0477(1996)077<0437:tnyrp>2.0.co;2

Kim, J. S., & Jain, S. (2010). High-resolution streamflow trend analysis applicable to annual decision calendars: A western United States case study. *Climatic Change*, *102*(3–4), 699–707. https://doi.org/10.1007/s10584-010-9933-3

Knowles, N., Dettinger, M. D., & Cayan, D. R. (2006). Trends in snowfall versus rainfall in the western United States. *Journal of Climate*, *19*(18), 4545–4559. https://doi.org/10.1175/JCLI3850.1

Koster, R. D., Suarez, M. J., Ducharne, A., Stieglitz, M., & Kumar, P. (2000). A catchment-based approach to modeling land surface processes in a general circulation model: 1. Model structure. *Journal of Geophysical Research*, *105*(D20), 24,809–24,822. https://doi.org/10.1029/2000JD900327

Li, D., Wrzesien, M. L., Durand, M., Adam, J., & Lettenmaier, D. P. (2017). How much runoff originates as snow in the western United States, and how will that change in the future? *Geophysical Research Letters*, *44*, 6163–6172. https://doi.org/10.1002/2017GL073551

Liang, X., Lettenmaier, D. P., Wood, E. F., & Burges, S. J. (1994). A simple hydrologically based model of land surface water and energy fluxes for general circulation models. *Journal of Geophysical Research*, *99*(D7), 14,415–14,428. https://doi.org/10.1029/94JD00483

Livneh, B., Rosenberg, E. A., Lin, C., Nijssen, B., Mishra, V., Andreadis, K. M., et al. (2013). A long-term hydrologically based dataset of land surface fluxes and states for the conterminous United States: Update and extensions. *Journal of Climate*, *26*(23), 9384–9392. https://doi.org/10.1175/JCLI-D-12-00508.1

Maurer, E. P., Brekke, L., Pruitt, T., & Duffy, P. B. (2007). Fine-resolution climate projections enhance regional climate change impact studies. *Eos, Transactions American Geophysical Union*, *88*(47), 504–504. https://doi.org/10.1029/2007EO470006

Maurer, E. P., Wood, A. W., Adam, J. C., Lettenmaier, D. P., & Nijssen, B. (2002). A long-term hydrologically based dataset of land surface fluxes and states for the conterminous United States. *Journal of Climate*, *15*(22), 3237–3251. https://doi.org/10.1175/1520-0442(2002)015%3C3237:althbd%3E2.0.co;2

Milly, P. C., & Dunne, K. A. (2020). Colorado River flow dwindles as warming-driven loss of reflective snow energizes evaporation. *Science*, *367*(6483), 1252–1255. https://doi.org/10.1126/science.aay9187

Monteith, J. L. (1965). Evaporation and environment. In *Symposia of the society for experimental biology* (Vol. 19, pp. 205–234). Cambridge: Cambridge University Press (CUP).

Mote, P. W., Hamlet, A. F., Clark, M. P., & Lettenmaier, D. P. (2005). Declining mountain snowpack in western North America. *Bulletin of the American Meteorological Society*, *86*(1), 39–50. https://doi.org/10.1175/BAMS-86-1-39

Mote, P. W., Li, S., Lettenmaier, D. P., Xiao, M., & Engel, R. (2018). Dramatic declines in snowpack in the western US. *Npj Climate and Atmospheric Science*, *1*(1), 2. https://doi.org/10.1038/s41612-018-0012-1

Niu, G. Y., Yang, Z. L., Mitchell, K. E., Chen, F., Ek, M. B., Barlage, M., et al. (2011). The community Noah land surface model with multiparameterization options (Noah-MP): 1 Model description and evaluation with local-scale measurements. *Journal of Geophysical Research*, *116*, D12109. https://doi.org/10.1029/2010JD015139

Pierce, D. W., Kalansky, J. F., & Cayan, D. R. (2018). *Climate, drought, and sea level rise scenarios for California's fourth climate change assessment*. La Jolla, CA: Division of Climate, Atmospheric Sciences, and Physical Oceanography Scripps Institution of Oceanography, California Energy Commission.

Reclamation. (2014). *Downscaled CMIP3 and CMIP5 climate and hydrology projections: Release of hydrology projections, comparison with preceding information, and summary of user needs*. Denver, CO: U.S. Department of the Interior, Bureau of Reclamation, Technical Services Center. Retrieved from https://gdo-dcp.ucllnl.org/downscaled_cmip_projections/techmemo/downscaled_climate.pdf

Rupp, D. E., Abatzoglou, J. T., Hegewisch, K. C., & Mote, P. W. (2013). Evaluation of CMIP5 20th century climate simulations for the Pacific Northwest USA. *Journal of Geophysical Research: Atmospheres*, *118*, 10,884–10,906. https://doi.org/10.1002/jgrd.50843

Sankarasubramanian, A., Vogel, R. M., & Limbrunner, J. F. (2001). Climate elasticity of streamflow in the United States. *Water Resources Research*, *37*(6), 1771–1781. https://doi.org/10.1029/2000WR900330

Stewart, I. T., Cayan, D. R., & Dettinger, M. D. (2005). Changes toward earlier streamflow timing across western North America. *Journal of Climate*, *18*(8), 1136–1155. https://doi.org/10.1175/JCLI3321.1

The U.S. Bureau of Reclamation (USBR). (2018). https://www.usbr.gov/lc/region/g4000/NaturalFlow/current.html

UMD vegetation classification scheme. (2020). https://ldas.gsfc.nasa.gov/nldas/vegetation-parameters

Vano, J. A., Das, T., & Lettenmaier, D. P. (2012). Hydrologic sensitivities of Colorado River runoff to changes in precipitation and temperature. *Journal of Hydrometeorology*, *13*(3), 932–949. https://doi.org/10.1175/jhm-d-11-069.1

Vano, J. A., & Lettenmaier, D. P. (2014). A sensitivity-based approach to evaluating future changes in Colorado River discharge. *Climatic Change*, *122*(4), 621–634. https://doi.org/10.1007/s10584-013-1023-x

Vano, J. A., Nijssen, B., & Lettenmaier, D. P. (2015). Seasonal hydrologic responses to climate change in the Pacific northwest. *Water Resources Research*, *51*, 1959–1976. https://doi.org/10.1002/2014WR015909

Wu, H., Kimball, J. S., Li, H., Huang, M., Leung, L. R., & Adler, R. F. (2012). A new global river network database for macroscale hydrologic modeling. *Water Resources Research*, *48*, W09701. https://doi.org/10.1029/2012WR012313

Xiao, M., Gao, M., Vogel, R. M., & Lettenmaier, D. P. (2020). Runoff and evapotranspiration elasticities in the Western US: Are they consistent with Dooge's complementary relationship? *Water Resources Research*, *56*, e2019WR026719. https://doi.org/10.1029/2019WR026719

Xiao, M., Udall, B., & Lettenmaier, D. P. (2018). On the causes of declining Colorado River streamflows. *Water Resources Research*, *54*, 6739–6756. https://doi.org/10.1029/2018WR023153

Yang, Y., Roderick, M. L., Zhang, S., McVicar, T. R., & Donohue, R. J. (2019). Hydrologic implications of vegetation response to elevated CO_2 in climate projections. *Nature Climate Change*, *9*(1), 44–48. https://doi.org/10.1038/s41558-018-0361-0

Yang, Z. L., Niu, G. Y., Mitchell, K. E., Chen, F., Ek, M. B., Barlage, M., et al. (2011). The community Noah land surface model with multiparameterization options (Noah-MP): 2 Evaluation over global river basins. *Journal of Geophysical Research*, *116*, D12110. https://doi.org/10.1029/2010JD015140